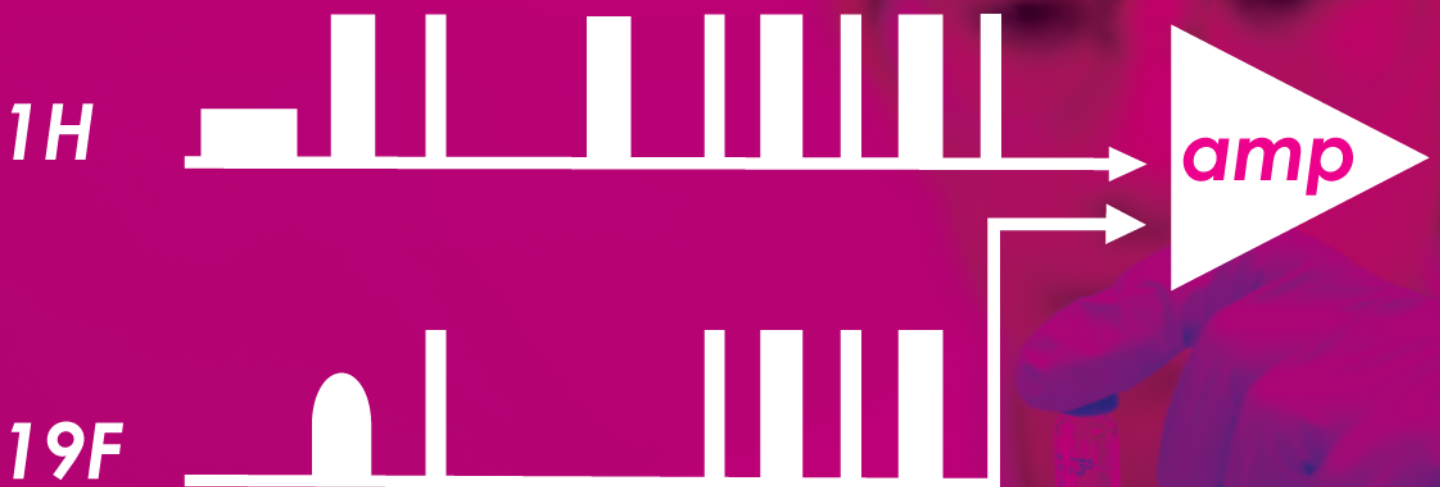


# Unlock the Potential of Multi-Resonance Experiments



*Download the Guide*

*RF pulse trains*



# Charting the solid-state NMR signals of polysaccharides: A database-driven roadmap

Wancheng Zhao | Debkumar Debnath | Isha Gautam |  
Liyanage D. Fernando | Tuo Wang 

Department of Chemistry, Michigan State University, East Lansing, Michigan, USA

## Correspondence

Tuo Wang, Department of Chemistry, Michigan State University, 578 S. Shaw Ln, East Lansing, MI 48824, USA.  
Email: wangtu01@msu.edu

## Funding information

National Science Foundation, Grant Numbers: MCB-2308660; DBI-2019046; DMR-2128556.

## Abstract

Solid-state nuclear magnetic resonance (ssNMR) measurements of intact cell walls and cellular samples often generate spectra that are difficult to interpret due to the presence of many coexisting glycans and the structural polymorphism observed in native conditions. To overcome this analytical challenge, we present a statistical approach for analyzing carbohydrate signals using high-resolution ssNMR data indexed in a carbohydrate database. We generate simulated spectra to demonstrate the chemical shift dispersion and compare this with experimental data to facilitate the identification of important fungal and plant polysaccharides, such as chitin and glucans in fungi and cellulose, hemicellulose, and pectic polymers in plants. We also demonstrate that chemically distinct carbohydrates from different organisms may produce almost identical signals, highlighting the need for high-resolution spectra and validation of resonance assignments. Our study provides a means to differentiate the characteristic signals of major carbohydrates and allows us to summarize currently undetected polysaccharides in plants and fungi, which may inspire future investigations.

## KEYWORDS

<sup>13</sup>C, carbohydrate, cell wall, cellulose, chitin, glucan, hemicellulose, pectin, solid-state NMR, xylan

## 1 | INTRODUCTION

Polysaccharides are high molecular weight biopolymers that typically consist of hundreds to thousands of sugar units. Elucidating the structure of complex carbohydrates with solid-state NMR (ssNMR) spectroscopy is a challenging task. Early pioneers in this field explored the use of different ssNMR methods, such as one-dimensional (1D) experiments for identifying the structure and quantifying the content of carbohydrate polymers and

allomorphs, and Rotational Echo Double Resonance (REDOR) and multidimensional correlation techniques for revealing polymer cross-linking and spatial proximities.<sup>1–6</sup> There has been a substantial increase in high-resolution ssNMR data that rely on <sup>13</sup>C and <sup>15</sup>N 2D/3D correlation experiments,<sup>7–9</sup> as well as <sup>1</sup>H detection,<sup>10–12</sup> to provide detailed insights into the structure and function of carbohydrates in a variety of living organisms.

Recent high-resolution ssNMR studies have led to numerous conceptual breakthroughs, including but not

This is an open access article under the terms of the [Creative Commons Attribution](https://creativecommons.org/licenses/by/4.0/) License, which permits use, distribution and reproduction in any medium, provided the original work is properly cited.

© 2023 The Authors. *Magnetic Resonance in Chemistry* published by John Wiley & Sons Ltd.

limited to the identification of cellulose-pectin spatial contacts in the primary plant cell walls (mostly the seedlings),<sup>13–16</sup> the conformation-dependent function of xylan in associating with lignin and cellulose in the secondary cell walls of grasses and woody stems,<sup>17–22</sup> the multi-layered assembly of chitin and glucans in fungal cell walls that provide remarkable structural dynamics to support microbial survival,<sup>23–28</sup> as well as the quantification of dynamically heterogeneous carbohydrate components in algal cells and bacterial cell wall and biofilms.<sup>29–33</sup> There is also a growing interest in utilizing ssNMR techniques for the characterization of carbohydrate-based materials, including hydrogels.<sup>34,35</sup>

By taking advantage of the repetitive nature of monosaccharides in a polysaccharide, the structural view of these polymers can be simplified, and their spectral features can be explored. Currently, there are five distinct structural variations of carbohydrates that can be closely tracked in the solid-state, which include the variation in covalent linkages, the compositional differences in cell walls and monosaccharide units that form polysaccharides, the conformational distribution of native polysaccharides, the spatial assembly, and the chemical modifications such as methylation and methyl esterification, as documented in a recent review article.<sup>36</sup> The majority of existing ssNMR studies depict polysaccharides in a simplified manner, reducing their complex structures to symbolic representations and only highlighting the most significant constituents showing strong signals.<sup>7</sup> While this approach enables researchers to concentrate on the primary polysaccharides found in a sample, it overlooks the many sparsely distributed molecules, minor side chains, and irregular substitutions, which may also contribute significantly to the structural stability and functional properties of both the polysaccharide and the cell wall.

In 2020, a complex carbohydrate magnetic resonance database (CCMRD) was established to accommodate the prolific growth of datasets in the upcoming years.<sup>37</sup> Upon its inception, the small-scale database contained 420 entries of high-resolution ssNMR data on carbohydrates. As of early 2023, the number of entries has increased to approximately 850. The database facilitates data search using single or paired chemical shifts, polysaccharide names, and compound classes, and it also supports user deposition. This platform also serves as a vital preparatory step for implementing semi-automated tools to streamline spectral analysis and resonance assignment of carbohydrate systems in the future as the size of the dataset increases.

The present study aims to accomplish three objectives by utilizing the available data. First, we aim to

construct artificial NMR spectra of commonly employed experiments to summarize the polysaccharide signals present in plants and fungi, which is akin to the amino acid maps available for protein NMR.<sup>38</sup> Second, we will utilize these spectroscopic maps to identify the unique signals that can unequivocally recognize specific polysaccharides. Finally, we will provide a synopsis of the key factors currently constraining our ability and give an overview of the undetected carbohydrates that necessitate further exploration. The pursuit of these objectives intends to encourage the use of high-resolution ssNMR in carbohydrate characterization.

## 2 | MATERIALS AND METHODS

### 2.1 | Generation of simulated 2D spectra from chemical shift data

We used a dataset containing 569 entries of plant and fungal carbohydrates sourced from CCMRD<sup>37</sup> to construct artificial 2D NMR spectra. Each entry within the dataset comprised <sup>13</sup>C chemical shift data for a carbohydrate unit sourced from a peer-reviewed publication. These publications featured high-resolution solid-state NMR data, typically presented in the form of 2D or 3D correlation spectra. The raw <sup>13</sup>C chemical shift data were transformed into different scatter plots depending on the targeted type of 2D spectra following the protocol described below.

For the refocused INADEQUATE spectrum that exhibits through-bond correlations,<sup>4</sup> the signals of two directly bonded carbons were situated at coordinates ( $\delta_{Ca}$ ,  $\delta_{Ca} + \delta_{Cb}$ ) and ( $\delta_{Cb}$ ,  $\delta_{Ca} + \delta_{Cb}$ ) on the plot. Here,  $\delta_{Ca}$  and  $\delta_{Cb}$  denote the single-quantum (SQ) chemical shifts of carbon sites a and b, respectively, and these values were projected to the X-axis of the simulated plot, corresponding to the direct dimension ( $\omega_2$ ) of experimentally measured spectra. The sum of two SQ chemical shifts ( $\delta_{Ca} + \delta_{Cb}$ ) were projected to the Y-axis, which represents the value of the double-quantum (DQ) chemical shift of this pair of carbons, corresponding to the indirect dimension ( $\omega_1$ ) of experimentally measured spectra. Each pyranose unit is represented by 10 scatter dots based on the chemical shifts of six carbons, and an illustrative example is presented in Figure 1a, showcasing the distribution of these scatter dots for a glucose unit in cellulose. In comparison, each furanose unit will result in eight scatter dots, due to the lack of C5–C6 spin pair.

More scatter dots are needed for plotting 2D <sup>13</sup>C SQ–SQ correlation spectra, such as PDS/DARR, CORD,<sup>39</sup>

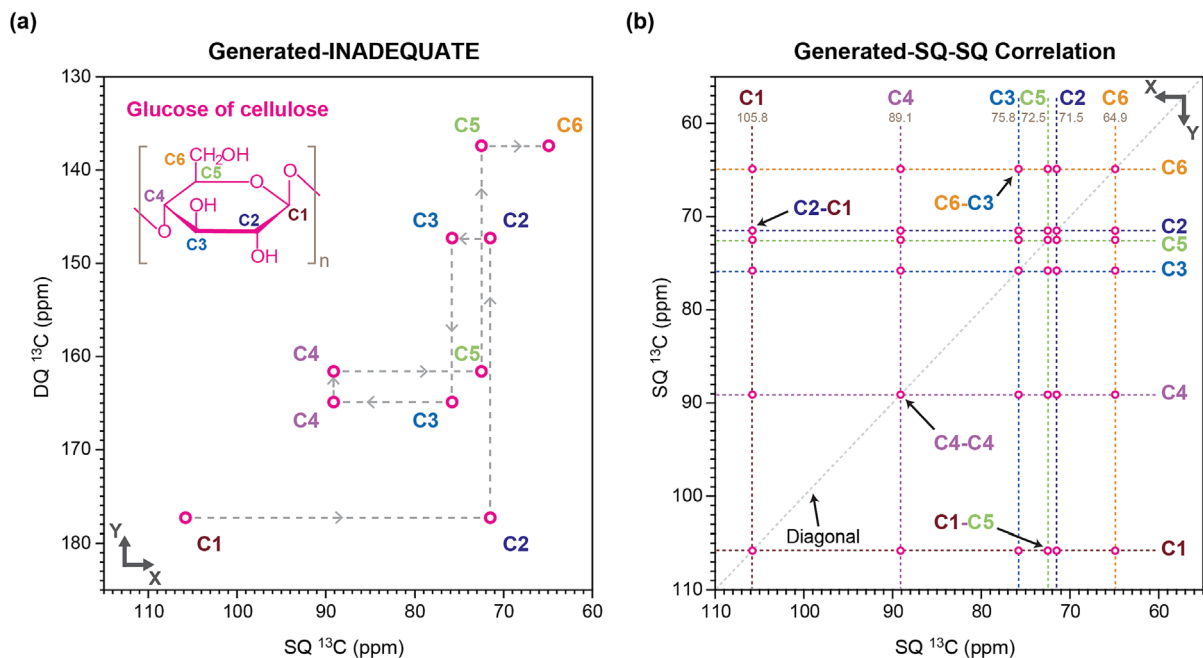


**FIGURE 1** Scatter plots of chemical shift values for a glucose unit of cellulose. The plots correspond to (a) DQ–SQ and (b) SQ–SQ  $^{13}\text{C}$  correlation experiments, with the former showing through-bond correlations and the latter showing all intramolecular through-space correlations. See Table S1 for comprehensive details on the dataset used to create these spectral projections.

and PAR.<sup>40</sup> This is because each carbon atom can potentially correlate with all the other carbons within the same monosaccharide unit. Each scatter dot now represents a distinct intramolecular cross peak, with the two coordinates representing the SQ chemical shifts of two carbons. When examining a pyranose, the anticipated SQ–SQ correlation spectrum consists of 36 derived data points, as illustrated in Figure 1b for a glucose unit of cellulose. Among these points, six are positioned along the spectral diagonal. In contrast, a furanose's spectrum contains 25 data points, with five residing on the diagonal. The chemical shift coordinates utilized in generating the scatter plots shown in Figure 1 are provided in Table S1.

Our analysis extended to encompass 412 entries from plant cell walls and 157 datasets from fungal cell walls obtained from CCMRD. Scatter plots were generated to depict both DQ–SQ and SQ–SQ correlation spectra for various sugar units. Subsequently, density maps were generated from these scatter plots using Kernel Density Estimate in Origin 2019b. These density maps provide an informative overview of the average trends represented by the scatter plots, allowing us to identify the specific regions and patterns related to different sugar units within 2D NMR spectra. Figures S1–S26 present individual plots for various plant and fungal carbohydrates. These figures can be used for direct comparison with experimental data, streamlining the analysis process.

## 2.2 | Sample preparation and packing

Three uniformly  $^{13}\text{C}$ -enriched samples were prepared for ssNMR measurement. These samples include the fungal culture of *Aspergillus fumigatus*, and the stems of two plant species: *Arabidopsis thaliana* and *Picea abies* (Norway spruce).<sup>21</sup> The fungal mycelium was cultivated for 2 weeks on a liquid minimal medium containing  $^{13}\text{C}$ -glucose as the only carbon source.<sup>26</sup> The spruce plant was grown within a closed atmosphere featuring 97 atom%  $^{13}\text{CO}_2$ . This controlled environment was maintained from germination until harvest, spanning approximately 4 months. Similarly,  $^{13}\text{C}$ -enriched *Arabidopsis* was grown in a custom-built transparent chamber for 4 weeks. The harvested fresh plant stems were cut into millimeter-scale pieces by razor blade for better distribution of mass during MAS.

Isotope-labeling is essential for acquiring high-resolution 2D/3D correlation spectra, particularly in dealing with the significant signal overlap encountered in cellular samples or complex biomaterials. Natural-abundance 2D  $^{13}\text{C}$ – $^{13}\text{C}$  correlation experiments of unlabeled samples becomes attainable with the utilization of the sensitivity-enhancing technique MAS-DNP, as recently demonstrated on lignocellulosic plant biomass,<sup>41–43</sup> fungal mycelia and conidia,<sup>44</sup> and functionalized cellulose materials.<sup>45–48</sup> However, it's important to note that at the low temperatures required for MAS-DNP, there is a significant sacrifice in spectral resolution.

Therefore, this technique is primarily employed when isotope-labeling presents challenges.

Around 30 mg of *A. fumigatus* was packed into a 3.2 mm MAS rotor and measured on an 800-MHz Bruker Avance Neo Spectrometer at National High Magnetic Field Laboratory using a 3.2-mm HCN MAS probe. Similarly, around 35 mg of *Arabidopsis* sample was packed into a 3.2-mm MAS rotor and measured on a 700-MHz Bruker Avance Neo Spectrometer at Louisiana State University using a 3.2-mm HCN MAS probe. For spruce, approximately 100 mg of material was packed into a 4-mm MAS rotor for measurement on a 400-MHz Bruker Avance spectrometer at Louisiana State University using a 4.0-mm HXY MAS probe.

## 2.3 | Solid-state NMR experiments

All experiments were performed with spinning speeds ranging from 10 to 13.5 kHz. The radiofrequency field strengths were set to 83.3 kHz for both  $^1\text{H}$  excitation and decoupling, and 62.5 kHz for  $^{13}\text{C}$  hard pulses. The recycle delays were 1.6–2.0 s. 2D experiments were recorded over durations of 4 to 30 h, while 1D data were collected in timeframes varying from 5 to 140 min. The 2D refocused J-INADEQUATE scheme was integrated with either direct polarization (DP) and short recycle delays of 1.8 s for the selective detection of mobile components, or with cross-polarization (CP) for the detection of rigid components. A 2D  $^{13}\text{C}$ - $^{13}\text{C}$  correlation experiment was also measured using the CORD scheme with a 53-ms recoupling period. Within each spectrum, both the sidechains and primary constituents of a polysaccharide, if they exhibit similar dynamics, were detected simultaneously. The acquisition time was 12–29 ms, and the evolution time for the indirect dimension of 2D experiments was 4–10 ms. The key parameters used in these ssNMR experiments are listed in Table S2.

Accurate experimental chemical shift data are essential for structural analysis.<sup>49</sup> All  $^{13}\text{C}$  NMR spectra are consistently referenced to the tetramethylsilane (TMS) scale by externally calibrating the  $\text{CH}_2$  signal of adamantane to 38.48 ppm at room temperature, which is a standard calibration procedure widely employed in solid-state NMR studies,<sup>50</sup> including carbohydrate research. In the chemical shift data deposited in CCMRD, NMR chemical shifts are only reported on the TMS scale, the information of which is included in each entry.<sup>37</sup> DSS scale is another reference scale that yields a  $^{13}\text{C}$  chemical shift difference of 2.0 ppm compared to the TMS scale. Chemical shifts reported on the DSS scale can be adjusted by subtracting 2.0 ppm for the purpose of comparison with data on the TMS scale, which has been reported in recent

studies of amyloid fibrils.<sup>51</sup> However, it finds primary usage in protein solid-state NMR and solution NMR studies. It should be noted that variations in chemical shifts may arise due to different calibration procedures employed by various research groups, as reported in recent cellulose studies.<sup>49</sup>

## 3 | RESULTS AND DISCUSSION

### 3.1 | Unique signals of different carbohydrates

Initial assignments of carbohydrate signals heavily rely on 2D  $^{13}\text{C}$  refocused INADEQUATE correlation experiments<sup>4</sup> that correlate DQ and SQ chemical shifts to obtain diagonal-free spectra. We extracted 412 plant carbohydrate entries and constructed artificial INADEQUATE spectra (Figure 2a). The scatter plots were derived from data deposited in CCMRD, with all through-bond correlations simulated for each carbohydrate unit. For example, for each hexose, the DQ and SQ chemical shifts were calculated for six spin pairs of C1–C2, C2–C3, C3–C4, C4–C5, and C5–C6, while the last spin pair is absent in each pentose. Furthermore, we created corresponding color-coded contour lines based on computed Kernel Density Estimate to represent the probability of different sugar residues in certain spectral regions. These maps included sugar residues found in context of a plant polysaccharide, such as the glucose units (Glc) found in cellulose and seven sugar residues commonly found in the matrix polysaccharides (hemicellulose and pectin), namely, xylose (Xyl), galacturonic acid (GalA), glucuronic acid (GlcA), arabinose (Ara), galactose (Gal), rhamnose (Rha), and mannose (Man) units (Figure 2b).

In particular, the Ara units are typically resolved by their C1–C2 spin pair, with unique DQ chemical shifts ranging from 188 to 198 ppm. Although the cellulose signals are tightly clustered with peaks from other carbohydrates, their C3–C4 and C4–C5 spin pairs can still be used as the starting point to track their signals. Xyl signals have a broad distribution but can be tracked using the C4–C5 spin pair:  $\alpha$ -linked Xyl has a unique DQ chemical shift at 130–135 ppm while  $\beta$ -linked Xyl typically shows up at 140–150 ppm, although the latter depends on the helical screw conformation. Rha can be unambiguously tracked starting from its C6, which is a methyl group, and the corresponding C5–C6 spin pair (Figure 2c). Acidic sugars, such as GalA and GlcA, rely on the spin pair between C5 and C6, which is the carbonyl group, for initiating the resonance assignment and tracking the other carbons within the same sugar unit.

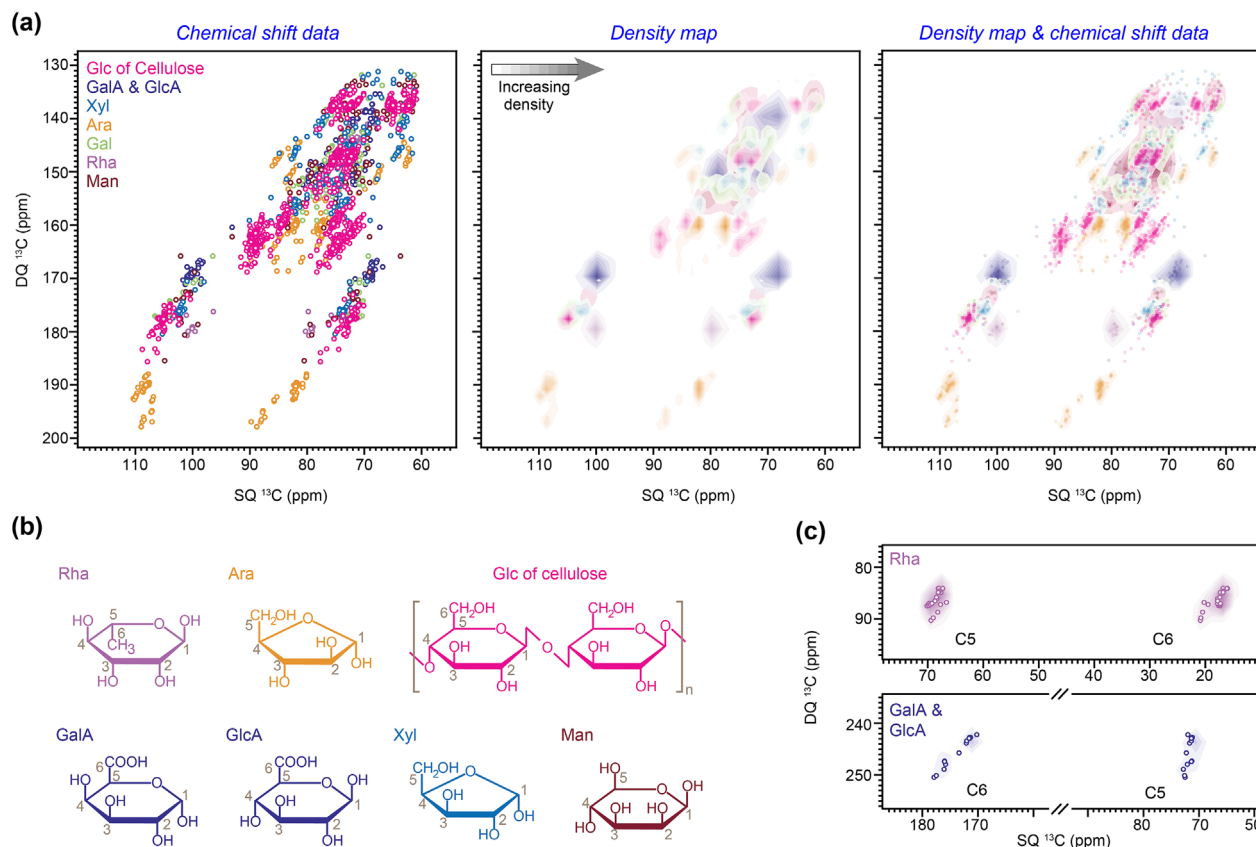


**FIGURE 2** Density map of plant polysaccharides projected into INADEQUATE spectra. (a)  $^{13}\text{C}$  chemical shift data of 412 datasets plotted as either scatter plot (left) or density map (middle), or both (right). The data of eight types of monosaccharide units were color coded. (b) Representative monosaccharide units with carbon numbers labeled. Two glucose units were shown for cellulose. (c) Unique spectral regions of the C5–C6 signals of Rha (top) and acidic residues (bottom), where the methyl and carbonyl groups can help to track the signals of these carbohydrates.

It should be noted that the chemical shift of the carbonyl groups in acidic sugars can vary significantly depending on the state of protonation, the deprotonation and ion coordination (e.g., with Calcium in HG and with Boron in RG-II),<sup>15,52</sup> as well as the degree of methyl esterification. Peak multiplicity in this spectral region has been consistently observed in many plant species, such as *Arabidopsis*, *Zea mays*, and *Brachypodium*,<sup>16,53–55</sup> with 176–178 ppm for carboxylate ( $-\text{COO}^-$  or  $-\text{COOH}$ ), 173–175 ppm for acetyl ( $-\text{OCOCH}_3$ ), and 170–172 ppm for methyl ester ( $-\text{COOCH}_3$ ). Due to the low bulk pKa of GalA ( $\sim 3.5$ ),<sup>56</sup> the carboxylate is in the deprotonated form under the near-neutral pH of most plant cell wall samples. However, the carboxylate signal vanishes GalA residues are neutralized during cell wall acidification, which has been observed at pH 4.0 in an *Arabidopsis* sample.<sup>57</sup> This further impedes GalA's capability to coordinate  $\text{Ca}^{2+}$  for crosslinking adjacent HG chains. Therefore, the pKa of these sugars and the pH of the samples being investigated should be considered and the carbonyl signals should be carefully tracked.

Signals of Gal residues are difficult to separate from the peaks of other sugar residues when using 2D  $^{13}\text{C}$ - $^{13}\text{C}$  correlation spectra; therefore, it requires special attention in analysis. The SQ chemical shift of carbon 4 site ( $\sim 78$  ppm) and the DQ chemical shifts of C3–C4 and C4–C5 (152–155 ppm) offer partial resolution in the refocused INADEQUATE spectrum, serving as an initial reference for Gal resonance assignment, especially for those in the mobile phase.<sup>55</sup> Proton-detection techniques such as 2D TOCSY and 3D HCC INEPT-TOCSY have been employed to distinguish Gal signals from other sugar residues in mobile matrix polysaccharides.<sup>10</sup>

We also presented these datasets as a 2D  $^{13}\text{C}$  SQ-SQ correlation spectrum, as shown in Figure 3. This spectrum encompasses all intramolecular cross-peaks, resembling the spectral patterns commonly observed with  $\sim 100$ -ms mixing periods under experimental schemes like CORD,<sup>39</sup> DARR/PDS, or other analogous approaches conducted at moderately slow magic-angle spinning (MAS) frequencies, for example, in the 10- to 20-kHz range. The simulated spectrum is more congested

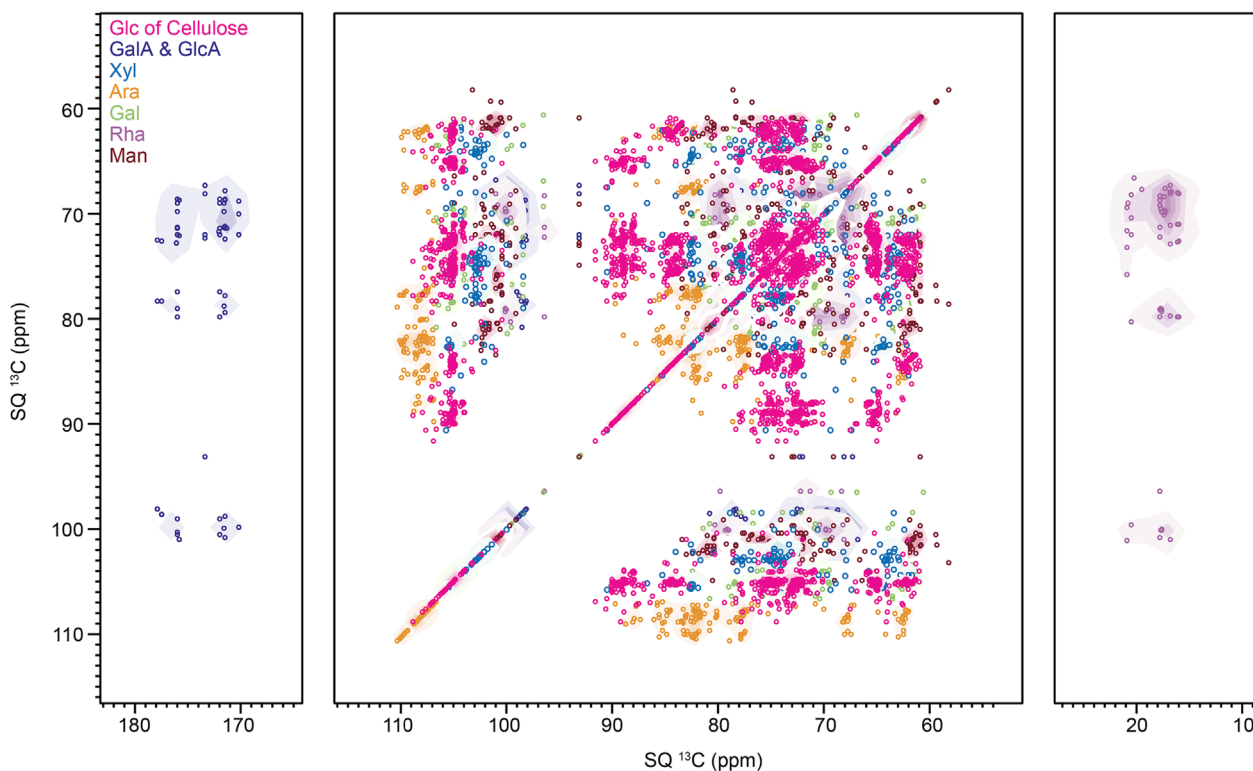


**FIGURE 3** Projected NMR signals of plant polysaccharides as the 2D SQ–SQ correlation spectra using the same datasets for plotting Figure 2.

than the INADEQUATE spectra shown earlier due to the presence of numerous multibond correlations. Nevertheless, discernable spectral regions are still available for almost every type of carbohydrate, except for Gal, where complementary techniques like the fast MAS INEPT spectra with  $^1\text{H}$  detection, as demonstrated in a recent study, may become necessary.<sup>10</sup>

### 3.2 | Reconstituted spectra for polysaccharide identification

Monosaccharide units can associate with others to form various polysaccharides. We synthesized artificial spectra to depict the potential range of chemical shift dispersion for polysaccharides (Figure 4a). The first spectrum cataloged all the signals identified in plant cellulose, which possesses a highly polymorphic structure characterized by up to seven types of Glc subforms within each plant sample.<sup>58</sup> The second spectrum encompassing Xyl and Ara signals, contained the spectra from various matrix polysaccharides, including hemicellulose arabinoxylan, pectic sidechain arabinan, as well as the sidechains of xyloglucan. Notably, the  $\alpha$ -Xyl units of xyloglucan and  $\beta$ -Xyl residues of xylan were not differentiated in this plot, but the distinction can be easily achieved, if

necessary. The third spectrum displayed the signals of acidic residues and Rha, which covered two primary pectic polymers: homogalacturonan (HG) and rhamnogalacturonan-I (RG-I), as well as the GlcA sidechains of the hemicellulose glucuronoxylan. The last spectrum displayed Gal and Man residues, which could be part of mannan polymers like galactoglucomannan (GGM), or the galactan sidechains of RG-I. The corresponding carbohydrate structures are summarized in Figure 4b.

The comparison of simulated carbohydrate maps with experimentally measured 2D spectra can aid in the initial evaluation of the sample and facilitate the identification of the most probable carbohydrates. As an example, we analyzed the refocused J-INADEQUATE spectrum of  $^{13}\text{C}$ -labeled *Arabidopsis* primary cell walls, which were measured using DP and short recycle delays of 1.8 s to select the mobile molecules with rapid  $^{13}\text{C}$ - $T_1$  relaxation (Figure 5a). Consequently, only dynamic matrix polysaccharides were detected, including the well-resolved signals of Rha, acidic sugars, and Ara from pectin, as well as the signature C4–C5 signals of  $\alpha$ -linked Xyl units from xyloglucan.

Ara units are distinguishable by their distinct signals falling within the DQ  $^{13}\text{C}$  chemical shift range of 188–200 ppm. Ara peaks are also evident in all other

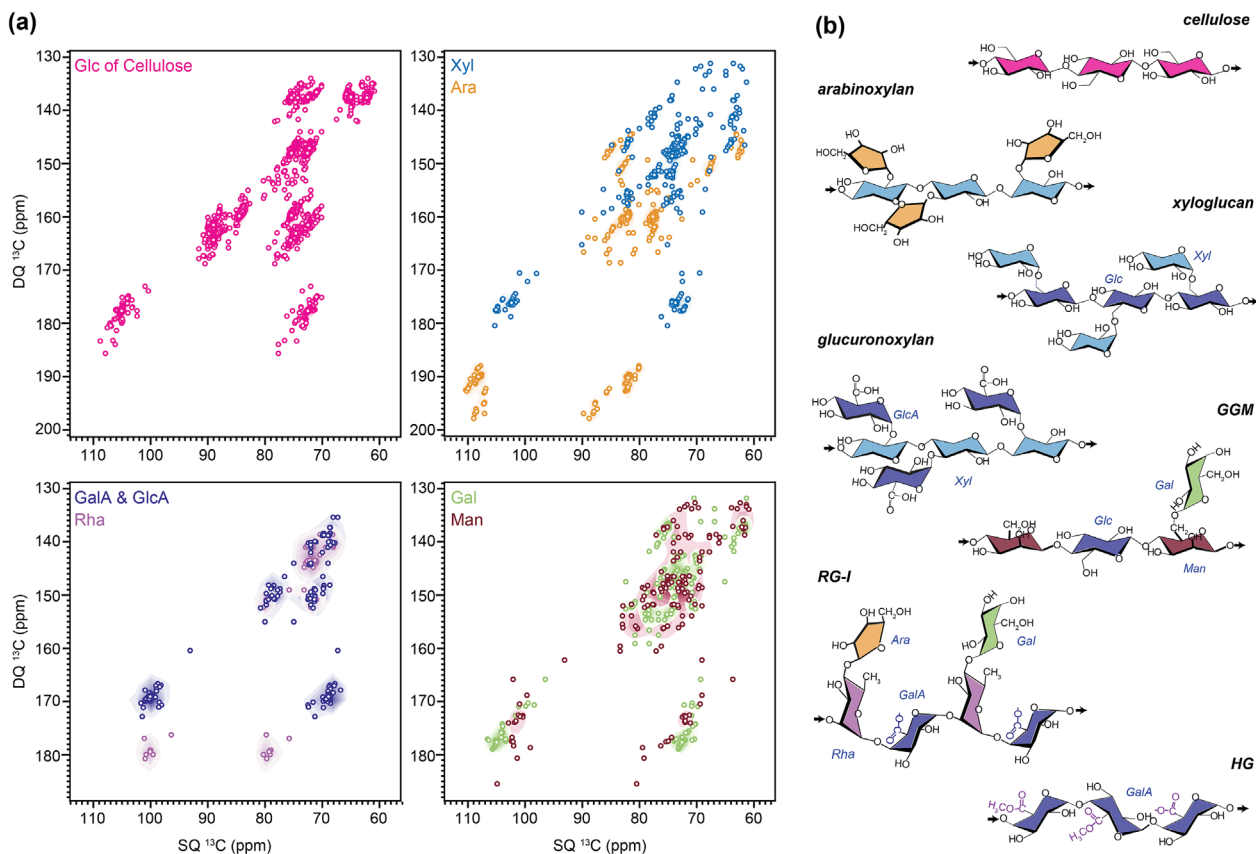


**FIGURE 4** Simulated NMR spectra of individual carbohydrate units. (a) Chemical shift dispersion and density maps of cellulose glucose units, Xyl, Ara, GalA and GlcA, Rha, Gal, and Man. (b) Simplified structure of polysaccharides containing these residues widely found in plant primary and secondary cell walls.

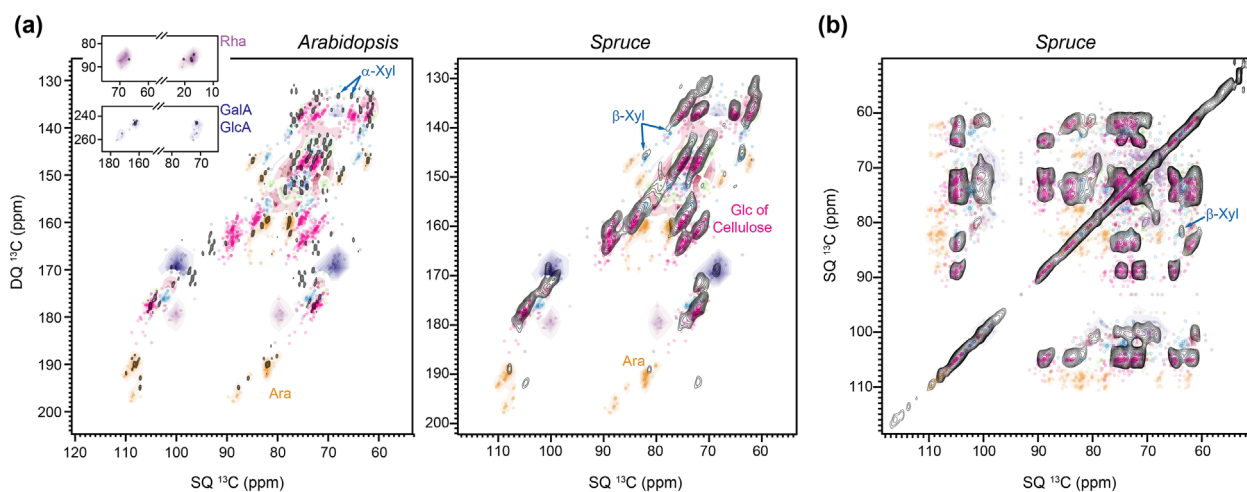


**FIGURE 5** Overlay of carbohydrate density map and experimental spectra for (a) refocused J-INADEQUATE and (b) 53-ms CORD spectra. The DP-based J-INADEQUATE spectrum measured on *Arabidopsis* primary cell walls, and the CP-based J-INADEQUATE and CORD experiments were conducted on spruce stems that are rich in secondary cell walls. *Arabidopsis* and spruce samples were measured on 700 and 400 MHz NMR spectrometers, respectively.

discernible spectral regions indicated by the yellow regions in the simulated density maps, which include the DQ chemical shift range of 160–170 ppm for C2–C3 and C3–C4, as well as the DQ chemical shift range of 145–155 ppm for C4–C5. These observations confirmed the presence of Ara residues in *Arabidopsis*. Similarly, the presence of Rha is verified by its characteristic C5–C6 signals, where C6 represents a methyl carbon, situated within the DQ chemical shift range of 80–90 ppm. The existence of acidic residues (GalA/GlcA) is substantiated by their unique signals with DQ chemical shifts extending beyond 240 ppm, corresponding to the covalently linked C5 and carbonyl group.

Cellulose is not detected in this spectrum, as evidenced by the absence of peaks in the magenta regions, where DQ chemical shifts typically fall within the range of 160–170 ppm, a characteristic range for C3–C4 and C4–C5 carbon pairs in cellulose. This outcome aligns with expectations since cellulose is a rigid component and is not found in this spectrum, which is designed to detect mobile components. Intensities are observed in other magenta regions, but these sharp signals originate from mobile polysaccharides exhibiting similar chemical shifts at these indistinguishable carbon positions.

The rigid portion of the spruce secondary cell wall was examined using  $^{13}\text{C}$  CP-based INADEQUATE and CORD experiments, where the spectra were dominated by cellulose signals (Figure 5a,b). Weak peaks were also spotted for the  $\beta$ -linked Xyl from xylan backbones and the Ara residues from xylan sidechains, as well as some Man signals from GGM. The  $\alpha$ -Xyl residues, which are indicative of xyloglucans, are not observed in this spectrum as shown by the absence of C4–C5 signals within the DQ chemical shift range of 130–136 ppm. This outcome is anticipated, considering that the spruce sample under examination is primarily composed of secondary cell wall component and the current spectrum selectively targets rigid polysaccharides, whereas xyloglucan, being partially mobile, exists in primary cell walls.

The use of carbohydrate fingerprints and the combination of selected datasets from certain glycans or organisms turned out to be an efficient approach for identifying polysaccharides, which should be applicable to both purified biopolymers and cellular samples. We have included a collection of individual scatter and density plots as Figures S1–S26 for the purpose of enabling direct comparisons with experimentally acquired spectra. This qualitative analysis will aid in identifying potential carbohydrates in the plant sample of interest as the initial step, which will require further validation or complete resonance assignment as subsequent procedures. As the *Arabidopsis* and spruce spectra were collected on 400- to 700-MHz NMR instruments, it is evident that a

moderate-to-high magnetic field is adequate for the implementation of this method. A current limitation is the lack of quantitative methods to assess the probability of specific resonance assignments, a capability akin to what is available for proteins and small molecules.<sup>59,60</sup> Further development of new software and algorithms<sup>61,62</sup> will be essential.

### 3.3 | Plant carbohydrates evading detection

Many polysaccharides remain elusive to solid-state NMR detection, even for the polysaccharides in plants, which have been relatively well studied. Although xyloglucan (XyG) is the primary hemicellulose in the primary cell wall, most studies have to rely on its  $\alpha$ -Xyl sidechains to track XyG signals and examine interactions with other cell wall components.<sup>13,63</sup> Its  $\beta$ -1,4-glucan backbone, as well as the occasional substitutions of  $\beta$ -galactose (Gal) and  $\alpha$ -fucose (Fuc),<sup>64</sup> have not been unambiguously identified. The signals corresponding to the  $\beta$ -1,4-glucan backbones are predominantly shielded by the surface glucan chains of cellulose, which are chemically identical, while the Gal and Fuc residues are relatively scarce. In addition, the third abundant pectic polymer, RG-II, has not been detected in intact cell wall samples either. RG-II contains at least 12 sugar types with complex linkages and has a relatively lower content compared with HG and RG-I, making it very difficult to characterize.<sup>65,66</sup> Moreover, chemical data suggest that pectic polymers exist in integrated networks containing polysaccharides and proteoglycans and might be covalently interconnected and further crosslinked to other cell wall macromolecules such as hemicellulose and protein components.<sup>66–68</sup> At this moment, such structural features have not been recognized using intact cell walls. The integration of solid-state NMR analysis with functional genomics, incorporating engineered mutants that selectively remove individual carbohydrate components, holds promise for the unambiguous identification of previously unresolved polysaccharides. This approach has recently proven successful in fungal species, particularly in resolving the ambiguity associated with the identification of galactosaminogalactan (GAG) and galactomannan (GM) within the cell walls of *Aspergillus* species.<sup>25</sup> Augmenting this approach with MAS-DNP can further mitigate detection issues associated with the low levels of certain carbohydrate components, such as RG-II and the Gal and Fuc sidechains of xyloglucan. Improvement in 2D/3D correlation experiments to achieve better signal dispersion,<sup>69,70</sup> coupled with the assessment of  $^1\text{H}$  chemical shifts using ultrafast MAS

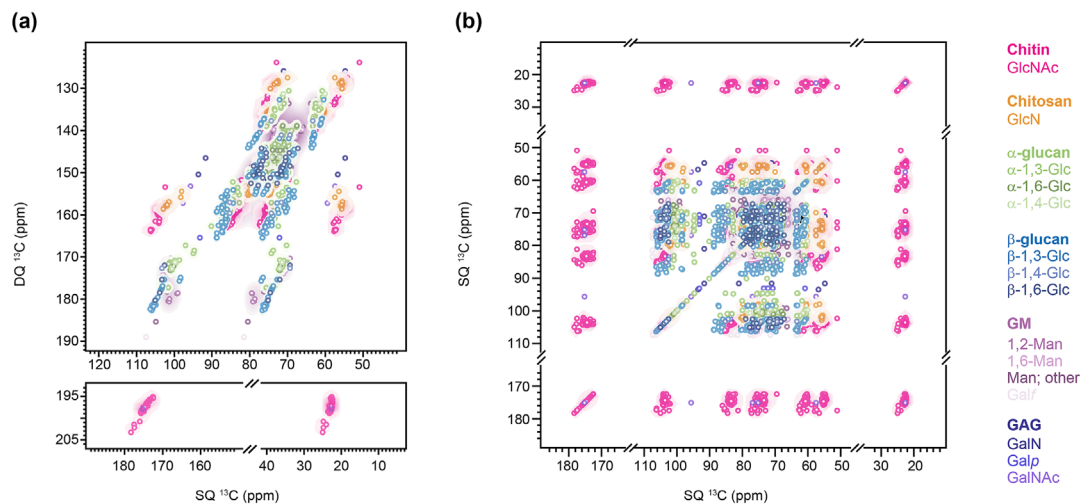


**FIGURE 6** Summary of  $^{13}\text{C}$  chemical shifts from fungal carbohydrates. The simulated spectra were presented as (a) DQ–DQ and (b) SQ–SQ correlation spectra. The current plot contains data from 157 entries, which is relatively limited and cannot efficiently represent the complex nature of fungal polysaccharides. The name of each polysaccharide is shown in bold followed by the monosaccharide units, including GlcNAc, GlcN, Glc, Man, Galf, GalN, Galp, and GalNAc.

techniques,<sup>10,71</sup> are poised to surmount the existing resolution limitations.

### 3.4 | Limited dataset of fungal carbohydrates

Fungal glycans have received inadequate attention, and most of the available data has been collected in the past 5 years, as summarized in Figure 6. We can unambiguously identify the signals from several amino sugars, such as the N-acetylglucosamine (GlcNAc) from chitin and the glucosamine (GlcN) from chitosan. Both chitin and chitosan have exhibited broad distribution owing to the high level of structural polymorphism in their crystallites.<sup>72,73</sup> However, the relationship between the polymorphism of chitin and chitosan and the diversity of chitin synthase gene families remains unclear.<sup>74</sup>  $\beta$ -glucans are prominent molecules widely distributed in different fungi, and have a high level of linkage complexity and can exist as different structures, such as linear  $\beta$ -1,3-glucan, branched  $\beta$ -1,3/1,6-glucan, linear  $\beta$ -1,3/1,4-glucan, and linear  $\beta$ -1,6-glucan, depending on the location within the cell wall and the fungal species being studied.<sup>75,76</sup> Different linkages can exist in the same fungi with variable percentages. For example, the  $\beta$ -glucans of yeast consist (~85%) of branched  $\beta$ -1,3-glucan, which contains ~3%  $\beta$ -1,3,6 interchain branching sites, with a smaller amount of linear  $\beta$ -1,6-glucans (~15%).<sup>76</sup> Meanwhile, the filamentous mold *Aspergillus fumigatus* also have predominantly branched  $\beta$ -1,3-glucan accounts with ~4%  $\beta$ -1,6 branching sites, but the minor component has changed

to  $\beta$ -1,3/1,4-glucan, which constitutes approximately 10% of the cell wall  $\beta$ -glucans in this species.<sup>75</sup> Solid-state NMR studies mainly focus on the function of  $\beta$ -1,3-glucan and ongoing research aims to identify the signals of each linkage type and relate them to their structural functions in the cell wall. Recent solid-state NMR studies have mainly focused on the function of  $\beta$ -1,3-glucan and ongoing research aims to identify the signals of each linkage type and relate them to their structural functions in the cell wall.

Recent studies have revealed the roles of  $\alpha$ -1,3-glucan in stabilizing the cell wall assembly, but information regarding the  $\alpha$ -1,4-linked glucose residue is lacking.<sup>77</sup> Other spotted monosaccharide units, such as galactofuranose (Galf), galactosamine (GalN), N-acetylgalactosamine (GalNAc), Man, and Fuc, belong to galactosaminogalactan (GAG), galactomannan (GM), phosphomannan, mannoproteins, and other minor cell wall polysaccharides, which can further complicated spectral analysis. The contribution of glycoproteins and lipid components to the cell wall architecture requires further investigation.<sup>78</sup>

Compared to their plant counterparts, fungal polysaccharides exhibit much higher structural diversity, and extensive solid-state NMR studies are necessary to document the carbohydrate signals across a wide range of fungal species to facilitate antifungal development and the biotechnology applications of these microorganisms. These endeavors may encompass the utilization of multi-dimensional correlation experiments involving  $^{13}\text{C}$ ,  $^{15}\text{N}$ , and  $^1\text{H}$  nuclear spins to elucidate the carbohydrate signals in significant human pathogenic species, such as

*Aspergillus*, *Candida*, and *Cryptococcus* species, as well as non-pathogenic species that could potentially be used for nutritional resources and biomaterials.<sup>28</sup>

### 3.5 | Distinct carbohydrates can have identical signals

Caution should be taken when utilizing NMR maps to investigate novel species with unknown composition. In certain instances, two distinct carbohydrates may demonstrate strictly overlapping signals, for example, between arabinofuranose (Araf) and Galf.<sup>25</sup> While Araf (typically called Ara in our studies) is a common sugar forming the side chains of pectin and hemicellulose in plants, Galf is a rare form of galactose and is sporadically identified in some fungal species, for example, as a constituent of the GM present in the cell wall.<sup>79–81</sup> Although Galf is a hexose and Ara is a pentose, both sugar units possess five-membered rings, resulting in identical <sup>13</sup>C chemical shifts in their first four carbons, with representative chemical shifts of approximately 108 ppm, 82 ppm, 77 ppm, and 84 ppm, respectively. The only unique signals of Galf in a 2D INADEQUATE spectrum come from its C5–C6 carbon pair, however, it showed up in a heavily crowded spectral region and cannot be utilized as a reliable tracker of molecules (Figure 7a). In a standard 1D spectrum, the sole distinctive signal for Galf, when compared to Araf, is the C5 signal at 69 ppm (Figure 7b). However, this peak falls within a densely populated region, making it impractical

for distinguishing signals from other carbohydrates. The occurrence of such indistinguishable spectral patterns between two chemically and structurally distinct monosaccharide units was unanticipated as we extend our reach of carbohydrate ssNMR and expand our knowledge and understanding of these complex biopolymers. Hence, it is essential to carefully consider the source of the samples being analyzed, be it from plants, fungi, or other organisms. In the case of a novel species, it becomes imperative to complement NMR analysis with the chemical assays that provide information on the linkage patterns and chemical composition of carbohydrate constituents. Moreover, the reliance on 1D spectra for analyzing previously uncharted samples should be minimized.

## 4 | CONCLUSIONS AND PERSPECTIVES

Significant advances have been made in solid-state NMR analysis of carbohydrates over the past decade, allowing us to identify key spectroscopic features of major plant and fungal glycans. It is critical to ensure that there is sufficient spectral resolution to track the minor differences in molecules, carefully track the full carbon connectivity in 2D/3D correlation spectra without missing any carbon in the linkage pattern, seek additional validation from other techniques, such as mass spectrometry, and cross-compare with mutants or other strains lacking

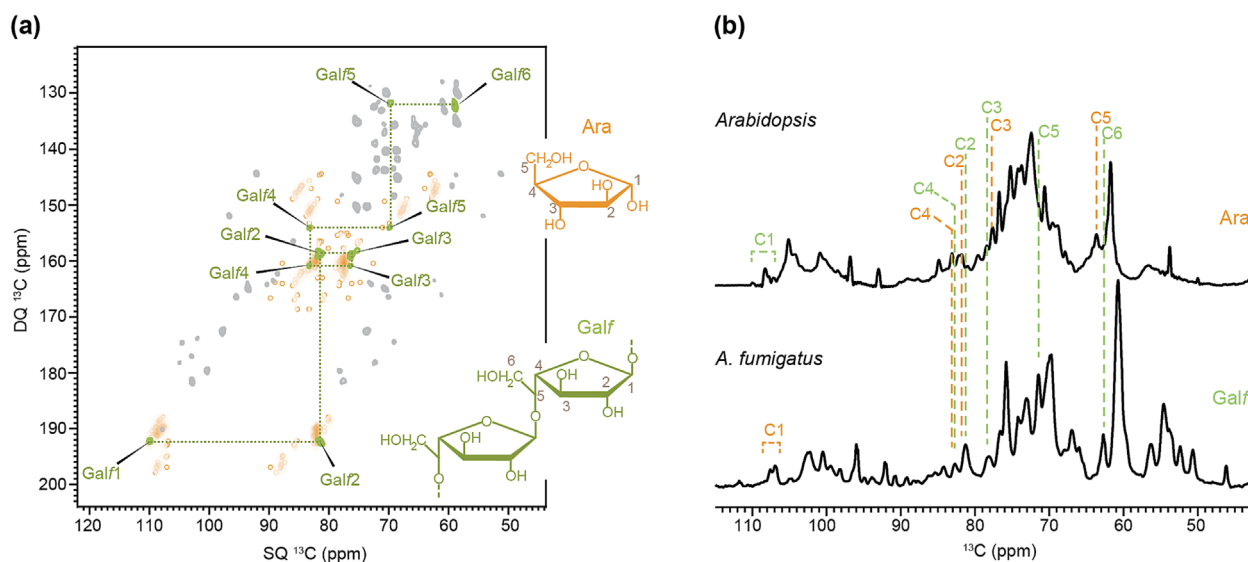


**FIGURE 7** Comparison of the NMR signals of Galf and Ara. (a) The C1–C2–C3–C4–C5 signals of Galf in the 2D DP refocused J-INADEQUATE spectrum of *A. fumigatus* falls within the expected signals for arabinose residues from plant cell walls. Only the C5–C6 carbon pair of Galf is unique. (b) Comparison of 1D <sup>13</sup>C quantitative DP spectrum measured on *Arabidopsis* (top) and *A. fumigatus* (bottom). Orange and green lines indicate the signals from Ara (only in *Arabidopsis*) and Galf residues (only in *A. fumigatus*), respectively.

the carbohydrate of interest. Further datasets are required before statistical analysis and automated tools can be developed to facilitate the analysis of these complex carbohydrate polymers. It is anticipated that tools similar to those already available for other molecules, such as the DEEP picker for protein 2D spectral deconvolution and peak picking, and the probabilistic assignment tool for organic crystals,<sup>59,82</sup> will lead to significant progress in solid-state glycoNMR.

## ACKNOWLEDGMENT

This work was supported by the National Science Foundation (NSF) MCB-2308660. Part of the NMR data was collected on a 700-MHz NMR spectrometer funded by NSF Major Research Instrumentation Program under the award number DBI-2019046. A portion of this work was performed at the National High Magnetic Field Laboratory, which is supported by National Science Foundation Cooperative Agreement No. DMR-2128556 and the State of Florida.

## CONFLICT OF INTEREST STATEMENT

The authors have no competing interests.

## PEER REVIEW

The peer review history for this article is available at <https://www.webofscience.com/api/gateway/wos/peer-review/10.1002/mrc.5397>.

## ORCID

Tuo Wang  <https://orcid.org/0000-0002-1801-924X>

## REFERENCES

- [1] T. Fukamizo, K. J. Kramer, D. D. Mueller, J. Schaefer, J. Carbow, G. S. Jacob, *Arch. Biochem. Biophys.* **1986**, *249*, 15.
- [2] J. Schaefer, E. O. Stejskal, C. F. Beard, *Plant Physiol.* **1975**, *55*, 1048.
- [3] M. Bardet, L. Emsley, M. Vincendon, *Solid State Nucl. Magn. Reson.* **1997**, *8*, 25.
- [4] A. Lesage, M. Bardet, L. Emsley, *J. Am. Chem. Soc.* **1999**, *121*, 10987.
- [5] G. Tong, Y. Pan, H. Dong, R. Pryor, G. E. Wilson, J. Schaefer, *Biochemistry* **1997**, *36*, 9859.
- [6] R. H. Atalla, D. L. Vanderhart, *Science* **1984**, *223*, 283.
- [7] N. Ghassemi, A. Poulhazan, F. Deligey, F. Mentink-Vigier, I. Marcotte, T. Wang, *Chem. Rev.* **2022**, *122*, 10036.
- [8] B. Reif, S. E. Ashbrook, L. Emsley, M. Hong, *Nat. Rev. Methods Primers* **2021**, *1*, 2.
- [9] W. Zhao, L. D. Fernando, A. Kirui, F. Deligey, T. Wang, *Solid State Nucl. Magn. Reson.* **2020**, *107*, 101660.
- [10] P. Phyo, M. Hong, *J. Biomol. NMR* **2019**, *73*, 661.
- [11] A. Safeer, F. Kleiburg, S. Bahri, D. Beriashvili, E. J. A. Veldhuizen, J. van Neer, M. Tegelaar, H. de Cock, H. A. B. Wosten, M. Baldus, *Chem. Euro. J.* **2022**, *29*, e202202616.
- [12] C. Bougault, I. Ayala, W. Vollmer, J. P. Simorre, P. Schanda, *J. Struct. Biol.* **2019**, *206*, 66.
- [13] M. Dick-Perez, Y. Zhang, J. Hayes, A. Salazar, O. A. Zabolina, M. Hong, *Biochemistry* **2011**, *50*, 989.
- [14] P. B. White, T. Wang, Y. B. Park, D. J. Cosgrove, M. Hong, *J. Am. Chem. Soc.* **2014**, *136*, 10399.
- [15] H. Temple, P. Phyo, W. Yang, J. J. Lyczakowski, A. Echevarria-Poza, I. Yakunin, J. P. Parra-Rojas, O. M. Terrett, S. Saez-Aguayo, R. Dupree, A. Orellana, M. Hong, P. Dupree, *Nat. Plants* **2022**, *8*, 656.
- [16] T. Wang, Y. B. Park, D. J. Cosgrove, M. Hong, *Plant Physiol.* **2015**, *168*, 871.
- [17] O. M. Terrett, J. J. Lyczakowski, L. Yu, D. Iuga, W. T. Franks, S. P. Brown, R. Dupree, P. Dupree, *Nat. Commun.* **2019**, *10*, 4978.
- [18] T. J. Simmons, J. C. Mortimer, O. D. Bernardinelli, A.-C. Pöpller, S. P. Brown, E. R. Deazevedo, R. Dupree, P. Dupree, *Nat. Commun.* **2016**, *7*, 13902.
- [19] R. Dupree, T. J. Simmons, J. C. Mortimer, D. Patel, D. Iuga, S. P. Brown, P. Dupree, *Biochemistry* **2015**, *54*, 2335.
- [20] X. Kang, A. Kirui, M. C. D. Widanage, F. Mentink-Vigier, D. J. Cosgrove, T. Wang, *Nat. Commun.* **2019**, *10*, 347.
- [21] A. Kirui, W. Zhao, F. Deligey, H. Yang, X. Kang, F. Mentink-Vigier, T. Wang, *Nat. Commun.* **2022**, *13*, 538.
- [22] Y. Gao, A. S. Lipton, Y. Wittmer, D. T. Murray, J. C. Mortimer, *Nat. Commun.* **2020**, *11*, 6081.
- [23] J. E. Kelly, C. Chrissian, R. E. Stark, *Solid State Nucl. Magn. Reson.* **2020**, *109*, 101686.
- [24] H. L. Ehren, F. V. W. Appels, K. Houben, M. A. M. Renault, H. A. B. Wösten, M. Baldus, *Cell Surf.* **2020**, *6*, 100046.
- [25] A. Chakraborty, L. D. Fernando, W. Fang, M. C. Dickwella Widanage, P. Wei, C. Jin, T. Fontaine, J. P. Latgé, T. Wang, *Nat. Commun.* **2021**, *12*, 6346.
- [26] X. Kang, A. Kirui, A. Muszynski, M. C. D. Widanage, A. Chen, P. Azadi, P. Wang, F. Mentink-Vigier, T. Wang, *Nat. Commun.* **2018**, *9*, 2747.
- [27] C. Chrissian, C. P.-C. Lin, E. Camacho, A. Casadevall, A. M. Neiman, R. E. Stark, *J. Fungi* **2020**, *6*, 329.
- [28] R. Pylkkanen, D. Werner, A. Bishoyi, D. Weil, E. Scoppola, W. Wagermaier, A. Safeer, S. Bahri, M. Baldus, A. Paananen, M. Penttila, G. Szilvay, P. Mohammadi, *Sci. Adv.* **2023**, *8*, ade5417.
- [29] R. Nygaard, J. A. H. Romaniuk, D. M. Rice, L. Cegelski, *Biophys. J.* **2015**, *108*, 1380.
- [30] A. A. Arnold, J. P. Bourgouin, B. Genard, D. E. Warschawski, R. Tremblay, I. Marcotte, *J. Biomol. NMR* **2018**, *70*, 123.
- [31] J. A. H. Romaniuk, L. Cegelski, *Philos. Trans. R. Soc. B* **2015**, *370*, 20150024.
- [32] A. Poulhazan, M. C. Dickwella Widanage, A. Muszynski, A. A. Arnold, D. E. Warschawski, P. Azadi, I. Marcotte, T. Wang, *J. Am. Chem. Soc.* **2021**, *143*, 19374.
- [33] C. Reichhardt, L. Cegelski, *Mol. Phys.* **2013**, *7*, 887.
- [34] M. El Hariri El Nokab, A. Lasorsa, K. O. Sebakhy, F. Pinccioni, P. C. A. van der Wel, *Food Hydrocol.* **2022**, *127*, 107500.
- [35] M. El Hariri El Nokab, P. C. A. van der Wel, *Carbohydr. Polym.* **2020**, *240*, 116276.
- [36] W. Zhao, F. Deligey, S. C. Shekar, F. Mentink-Vigier, T. Wang, *J. Magn. Reson.* **2022**, *341*, 107263.

- [37] X. Kang, W. Zhao, M. C. D. Widanage, A. Kirui, U. Ozdenvar, T. Wang, *J. Biomol. NMR* **2020**, *74*, 239.
- [38] K. J. Fritzsching, M. Hong, K. Schmidt-Rohr, *J. Biomol. NMR* **2016**, *64*, 115.
- [39] G. Hou, S. Yan, J. Trebosc, J. P. Amoureux, T. Polenova, *J. Magn. Reson.* **2013**, *232*, 18.
- [40] G. De Paepe, J. R. Lewandowski, A. Loquet, A. Bockmann, R. G. Griffin, *J. Chem. Phys.* **2008**, *129*, 245101.
- [41] W. Zhao, A. Kirui, F. Delige, F. Mentink-Vigier, Y. Zhou, B. Zhang, T. Wang, *Biotechnol. Biofuels* **2021**, *14*, 14.
- [42] J. Viger-Gravel, W. Lan, A. C. Pinon, P. Berruyer, L. Emsley, M. Bardet, J. Luterbacher, *J. Phys. Chem. C* **2019**, *123*, 30407.
- [43] F. A. Perras, H. Luo, X. Zhang, N. S. Mosier, M. Pruski, M. M. Abu-Omar, *J. Phys. Chem. A* **2017**, *121*, 623.
- [44] L. D. Fernando, M. C. Dickwella Widanage, S. C. Shekar, F. Mentink-Vigier, P. Wang, S. Wi, T. Wang, *J. Struct. Biol. X* **2022**, *6*, 100070.
- [45] F. Delige, M. A. Frank, S. H. Cho, A. Kirui, F. Mentink-Vigier, M. T. Swilius, B. T. Nixon, T. Wang, *Biomacromolecules* **2022**, *23*, 2290.
- [46] H. Takahashi, D. Lee, L. Dubois, M. Bardet, S. Hediger, G. De Paepe, *Angew. Chem., Int. Ed.* **2012**, *51*, 11766.
- [47] A. Kumar, B. Watbled, I. Baussanne, S. Hediger, M. Demeunynck, G. De Paepe, *Commun. Chem.* **2023**, *6*, 58.
- [48] P. Berruyer, M. Gericke, P. Moutzouri, D. Jakobi, M. Bardet, L. Karlson, S. Schantz, T. Heinze, L. Emsley, *Carbohydr. Polym.* **2021**, *262*, 117944.
- [49] D. H. Brouwer, J. G. Mikolajewski, *Cellulose* **2023**, *30*, 4827.
- [50] R. Hoffman, *J. Magn. Reson.* **2022**, *340*, 107231.
- [51] M. R. Elkins, T. Wang, M. Nick, H. Jo, T. Lemmin, S. B. Prusiner, W. F. DeGrado, J. Stohr, M. Hong, *J. Am. Chem. Soc.* **2016**, *138*, 9840.
- [52] A. Kirui, J. Du, W. Zhao, W. Barnes, X. Kang, C. T. Anderson, C. Xiao, T. Wang, *Carbohydr. Polym.* **2021**, *270*, 118370.
- [53] T. Wang, Y. Chen, A. Tabuchi, D. J. Cosgrove, M. Hong, *Plant Physiol.* **2016**, *172*, 2107.
- [54] T. Wang, A. Salazar, O. A. Zabolina, M. Hong, *Biochemistry* **2014**, *53*, 2840.
- [55] P. Phyto, T. Wang, S. N. Kiemle, H. O'Neill, S. V. Pingali, M. Hong, D. J. Cosgrove, *Plant Physiol.* **2017**, *175*, 1593.
- [56] R. Kohn, P. Kovac, *Chem. Pap.* **1978**, *32*, 478.
- [57] P. Phyto, Y. Gu, M. Hong, *Cellulose* **2018**, *26*, 291.
- [58] T. Wang, H. Yang, J. D. Kubicki, M. Hong, *Biomacromolecules* **2016**, *17*, 2210.
- [59] M. Cordova, M. Balodis, B. S. de Almeida, M. Ceriotti, L. Emsley, *Sci. Adv.* **2021**, *7*, abk2341.
- [60] K. J. Fritzsching, Y. Yang, K. Schmidt-Rohr, M. Hong, *J. Biomol. NMR* **2013**, *56*, 155.
- [61] Y. Yang, K. J. Fritzsching, M. Hong, *J. Biomol. NMR* **2013**, *57*, 281.
- [62] K. N. Hu, W. Qiang, R. Tycko, *J. Biomol. NMR* **2011**, *50*, 267.
- [63] M. Dick-Perez, T. Wang, A. Salazar, O. A. Zabolina, M. Hong, *Magn. Reson. Chem.* **2012**, *50*, 539.
- [64] H. V. Scheller, P. Ulvskov, *Annu. Rev. Plant Biol.* **2010**, *61*, 263.
- [65] B. L. Ridley, M. A. O'Neill, D. Mohnen, *Phytochemistry* **2001**, *57*, 929.
- [66] M. A. Atmodjo, Z. Hao, D. Mohnen, *Annu. Rev. Plant Biol.* **2013**, *64*, 747.
- [67] A. K. Biswal, M. A. Atmodjo, M. Li, H. L. Baxter, C. Geun Yoo, Y. Pu, Y. C. Lee, M. Mazarei, I. M. Black, J. Y. Zhang, H. Ramanna, A. L. Bray, Z. R. King, P. R. LaFayette, S. Pattathil, B. S. Donohoe, S. S. Mohanty, D. Ryno, K. Yee, O. A. Thompson, M. Rodriguez, A. Dumitrache, J. Natzke, K. Winkeler, et al., *Nat. Biotechnol.* **2018**, *36*, 249.
- [68] L. Tan, L. Zhang, I. M. Black, J. Glushka, B. Urbanowicz, C. Heiss, P. Azadi, *Carbohydr. Polym.* **2023**, *301*, 120340.
- [69] S. C. Shekar, W. Zhao, L. D. Fernando, I. Hung, T. Wang, *J. Magn. Reson.* **2022**, *336*, 107148.
- [70] S. Li, Y. Zhang, M. Hong, *J. Magn. Reson.* **2010**, *202*, 203.
- [71] S. Bahri, A. Safeer, A. Adler, H. Smedes, H.v. Ingen, M. Baldus, *J. Biomol. NMR* **2023**, *77*, 111.
- [72] L. D. Fernando, M. C. Dickwella Widanage, J. Penfield, A. S. Lipton, N. Washton, J. P. Latge, P. Wang, L. Zhang, T. Wang, *Front. Mol. Biosci.* **2021**, *8*, 727053.
- [73] C. K. S. Pillai, W. Paul, C. P. Sharma, *Prog. Polym. Sci.* **2009**, *34*, 641.
- [74] M. D. Lenardon, R. K. Whitton, C. A. Munro, D. Marshall, N. A. R. Gow, *Mol. Microbiol.* **2007**, *66*, 1164.
- [75] J.-P. Latgé, *Mol. Microbiol.* **2007**, *66*, 279.
- [76] J. Rui-Herrera, L. Ortiz-Castellanos, *Cell Surf.* **2019**, *5*, 100022.
- [77] C. H. Grun, F. Hochstenbach, B. Humbel, A. J. Verkleij, J. H. Sietsma, F. M. Klis, J. P. Kamerling, J. F. G. Vliegthart, *Glycobiology* **2005**, *15*, 245.
- [78] N. A. R. Gow, M. D. Lenardon, *Nat. Rev. Microbiol.* **2022**, *21*, 248.
- [79] T. Fontaine, J. P. Latgé, *J. Fungi* **2020**, *6*, 283.
- [80] J. P. Latge, *Med. Mycol.* **2009**, *47*, S104.
- [81] C. Heiss, M. L. Skowrya, H. Liu, J. S. Klutts, Z. Wang, M. Williams, D. Srikanta, S. M. Beverley, P. Azadi, T. L. Doering, *J. Biol. Chem.* **2013**, *288*, 10994.
- [82] D. W. Li, A. L. Hansen, C. Yuan, L. Bruschweiler-Li, R. Bruschweiler, *Nat. Commun.* **2021**, *12*, 5229.

## SUPPORTING INFORMATION

Additional supporting information can be found online in the Supporting Information section at the end of this article.

**How to cite this article:** W. Zhao, D. Debnath, I. Gautam, L. D. Fernando, T. Wang, *Magn Reson Chem* **2023**, *1*. <https://doi.org/10.1002/mrc.5397>